A Terminal Fluoride Ligand Generates Axial Magnetic Anisotropy in Dysprosium Complexes

Lucie Norel, Lucy E. Darago, Boris Le Guennic, Khetpakorn Chakarawet, Miguel I. Gonzalez, Jacob H. Olshansky, Stéphane Rigaut, Jeffrey R. Long

10.1002/anie.201712139

COMMUNICATION

A Terminal Fluoride Ligand Generates Highly Axial Magnetic Anisotropy in Dysprosium Complexes

Dr. Lucie Norel,*[a][b] Lucy E. Darago,[a] Dr. Boris Le Guennic,[b] Khetpakorn Chakarawet,[a] Miguel I. Gonzalez,[a] Dr. Jacob H. Olshansky,[a] Prof. Stéphane Rigaut[b] and Prof. Jeffrey R. Long*[a]

Abstract: The first dysprosium complexes with a terminal fluoride ligand are obtained as air-stable compounds. The strong, highly electrostatic dysprosium–fluoride bond generates a large axial crystal field splitting of the J = 15/2 ground state, as evidenced by high-resolution luminescence spectroscopy and correlated with the single-molecule magnet behavior through experimental magnetic susceptibility data and *ab initio* calculations.

Since the discovery of single-molecule magnets,[1] the search for improved properties, in particular enhanced thermal barriers to magnetic relaxation and magnetic blocking temperatures, has driven the development of new complexes with magnetic properties customized by coordination environment.[2] This approach has been widely applied for mononuclear lanthanide complexes, wherein the barrier to slow magnetic relaxation originates from splitting of the ground state by the crystal field.[3] Here, manipulation of the crystal field provides a basis for improving single-molecule magnet properties, as analyzed by applying electrostatic models or more elaborate quantum chemistry calculations.[4]

In the case of dysprosium(III), a linear two-coordinate complex provides the ideal coordination environment, with the two ligands serving as anionic point charges that preferably reside as close to the metal center as possible in order to maximize crystal-field splitting.[5] Approximating this synthetically challenging geometry with pseudo-linear complexes possessing strongly-donating axial ligands,[6] such as in the pentagonal bipyramidal complex $[Dy(^tBuO)_2(py)_5]^+$[6b] and sandwich complexes such as $[(Cp^{ttt})_2Dy]^+$,[7] prompt a strong axiality of nearly all of the crystal-field-split magnetic doublets. This axiality can lead to impressive relaxation barriers of U_{eff} > 1200 cm^{-1}, and, for the latter complex, a record hysteresis temperature of 60 K. In spite of their exceptional magnetic behavior, these complexes are unstable in the presence of air and water, which limits their utility beyond the lab setting. In pursuit of ligands that would engender a similar or even stronger crystal field splitting while showing greater stability to air and water, we selected terminal fluoride as a candidate. We envisioned that a Dy–(η^1-F) or (η^1-F)–Dy–(η^1-F) unit stabilized by an appropriate ligand environment would have strong axial anisotropy based on the dominant dysprosium–fluoride electrostatic interaction. Indeed, *ab initio* calculations performed on the hypothetical $[Dy–F]^{2+}$ and $[F–Dy–F]^+$ units predict a $|M_J>$ = ±15/2 ground state stabilized by several hundreds of wavenumbers, even with a Dy–F distance arbitrarily fixed to a likely overestimated distance of 2.5 Å.[5a]

Synthesis of an idealized low-coordinate lanthanide complex or even heteroleptic complexes with an η^1-F ligand, however, is challenging because of the tendency of the fluoride ligand to either coordinate in a bridging fashion or to form the stable and insoluble LnF_3 compounds.[8] Among structurally-characterized mononuclear lanthanide complexes with a terminal fluoride ligand[9] is a tris(3-(2-pyridyl)pyrazolyl)hydroborate (Tp^{py}) complex $[Eu(Tp^{py})F(MeOH)_2]^+$ in which the hexadentate Tp^{py} ligand prevents unwanted aggregation of lanthanide moieties.[10] We thus investigated dysprosium(III) analogues of this type to evaluate whether a single terminal fluoride donor is sufficient to create a large axial crystal field, thereby engendering single-molecule magnet behavior. Here, we report the synthesis of two air-stable compounds, $[Dy(Tp^{py})F(dioxane)](PF_6)$ (**1**) and $[Dy(Tp^{py})F(pyridine)_2](PF_6)$ (**2**), and the precise determination of their $^6H_{15/2}$ ground state crystal field splittings by low-temperature luminescence measurements.[11] Dynamic magnetic susceptibility studies reveal large energy barriers to slow magnetic relaxation that correlate well with the axial crystal field splittings observed by luminescence and predicted by *ab initio* calculations.

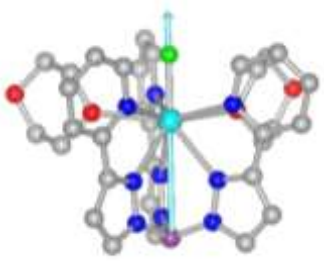

Figure 1. View of one cationic molecular unit forming the one-dimensional chain in compound **1** as determined from single-crystal X-ray diffraction data at 100 K, together with the calculated magnetic anisotropy axis (light blue arrow). Grey, blue, red, purple, green, and light blue spheres represent C, N, O, B, F and Dy atoms, respectively; H atoms are omitted for clarity.

Compound **1** and its yttrium analog **1-Y** were synthesized through a modification of a previously reported procedure[10a] and crystallized by slow diffusion of dioxane, affording a 1D coordination compound with bridging dioxane ligands in 36% yield. Complex **2** (resp. **2-Y**) was obtained by dissolution of **1**

[a] L. E. Darago, K. Chakarawet, M. I. Gonzalez, Dr. J. H. Olshansky, Prof. Dr. J. R. Long
Department of Chemistry,
University of California, Berkeley, California 94720, United States
E-mail: jrlong@berkeley.edu
[b] Dr. B. Le Guennic, Dr. L. Norel, Prof. Dr. S. Rigaut
Institut des Sciences Chimiques de Rennes, UMR 6226 CNRS - Université de Rennes 1,
263 Avenue du Général Leclerc, 35042 Rennes Cedex, France
E-mail: lucie.norel@univ-rennes1.fr,

Supporting information for this article is given via a link at the end of the document

(resp. **1-Y**) in pyridine and crystallization by aerial diffusion of petroleum ether in 40% yield. Detailed experimental procedures and full characterization of these complexes can be found in the Supporting Information. Upon dissolution in *d*^{4}-methanol, both **1-Y** and **2-Y** showed clean ^{1}H NMR and ^{19}F NMR spectra, corresponding to the species $[Y(Tp^{py})F(CD_3OD)_2]^+$ together with free dioxane (for **1-Y**) or pyridine (for **2-Y**), confirming complexes composition and purity. Notably, the ^{19}F NMR spectrum showed the expected Y–F coupling, with J_{Y-F} = 69.4 Hz.

Single-crystal X-ray diffraction structures obtained for the four compounds revealed that each metal ion is nine-coordinate with one terminal fluoride, the hexadentate Tp^{py} ligand, and two pyridine or dioxane ligands (see Figures 1 and S3-S5 and Table S1-S2). The resulting geometry is a capped square antiprism.[12] As expected, the fluoride ligand provides the shortest bond to the metal center, due to its hard Lewis base character. For instance, in compound **1**, the Dy–F distance is 2.094(4) Å and the next shortest bond distances occur between Dy and the nitrogen atoms of the pyrazolyl rings (Dy–N = 2.472(6) and 2.482(4) Å). The Dy–N(pyridine rings of the Tp^{py}) and Dy–O(dioxane) bond lengths are both longer than 2.53 Å. In the case of **1** (and **1-Y**), the metal sits on a mirror plane that includes one pyridylpyrazolyl arm of the Tp^{py} ligand. Owing to the bridging nature of the dioxane ligands, the compounds crystallize as one-dimensional chains, and in the case of **1** the intrachain Dy···Dy distance is 7.81 Å. In contrast, compounds **2** and **2-Y** are mononuclear and the coordination sphere is slightly more distorted due to π-stacking between pyridylpyrazolyl arms of adjacent complexes (Figure S5). The shortest Dy···Dy distance in **2** is 8.46 Å.

Emission spectra were measured on crystalline samples of **1** and **2**. For both compounds, two transitions could be observed at room temperature in the accessible range of our instrument, the energies of which correspond well with the expected values for the $^4F_{9/2} \rightarrow {}^6H_{15/2}$ (~480 nm, 20830 cm^{-1}) and $^4F_{9/2} \rightarrow {}^6H_{13/2}$ (~575 nm, 17390 cm^{-1}) transitions (Figure 2).[13] Liquid helium cooling substantially improved the spectral resolution, revealing eight (resp. seven) lines for the first (second) transition (Figures 3 and S6-S9), with each line corresponding to a transition to one of the eight (seven) doublets composing the $^6H_{15/2}$ ($^6H_{13/2}$) state. The absence of any hot band or additional feature in the low-temperature spectra, which usually complicates the analysis,[11b-h] makes the extraction of crystal field splitting energies for the ground states straightforward (Tables S4-S7). For **1** (resp. **2**), the total splitting of the $^6H_{15/2}$ ground state is 770 cm^{-1} (790 cm^{-1}) and the first and second excited doublets are situated 318 and 453 cm^{-1} (335 and 457 cm^{-1}) above the ground state doublet. The energy differences between the two compounds are minimal, indicating that the variation of the two equatorial ligands from O-donors to N-donors has only a small influence on the crystal field splitting, which is dominated by the dysprosium–fluoride interaction. The unambiguous assignment of all eight doublet energies of the $^6H_{15/2}$ ground state is quite rare,[11a, 11b] and is made possible here because both complexes combine bright emission with substantial crystal field splitting.

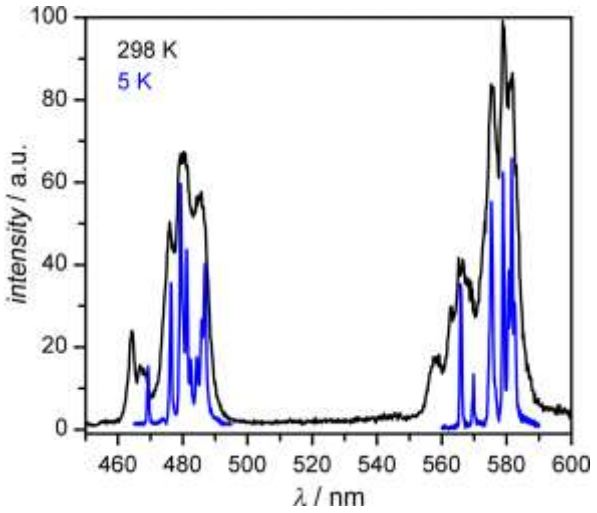

Figure 2. Emission spectrum of **1** recorded at room temperature (black line) and at 5 K (blue line) upon 280 nm excitation.

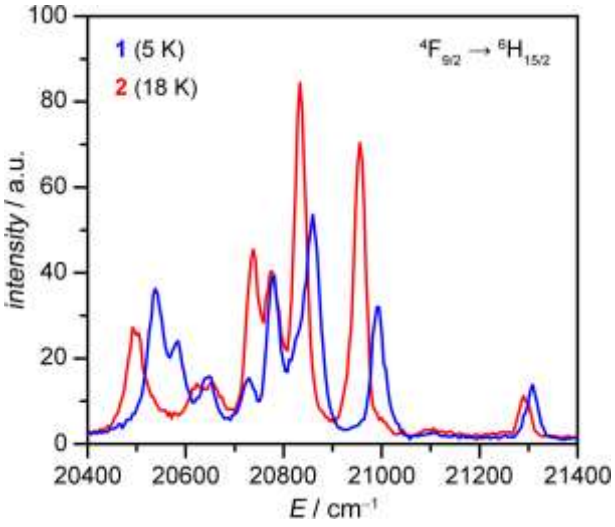

Figure 3. Luminescence spectra highlighting the ground state multiplet splitting for **1** (blue line, 5 K, 0.2 nm detection slit opening) and **2** (red line, 18 K, 0.4 nm detection slit opening) upon 280 nm excitation.

Ab initio calculations (see computational details in the Supporting Information) were performed based on the molecular structures of **1** and **2**, excluding the PF_6^- counterions and solvate molecules of crystallization. In both cases, the calculated splittings of the ground state are in excellent agreement with the luminescence spectra (Tables S14-S15). For example, in the case of **1**, the calculated total splitting of 778 cm^{-1} and the calculated first excited state energy of 297 cm^{-1} correspond well with the respective energy spacings of 770 cm^{-1} and 318 cm^{-1} determined from the luminescence experiment. Notably, the correlation is also very good between the calculated and experimental splittings of the $^6H_{13/2}$ state (Figure S27). As experimentally observed, the influence of the equatorial solvent ligands on the calculated ground state splitting is minimal. We were thus able to confidently assign the various magnetic

doublets of **1** based upon the *ab initio* results, with the ground state, first excited state, and second excited state assigned as rather pure $|M_J>$ = ±15/2± ,13/2 and ±11/2 states, respectively, while for the other components (3rd to 8th doublets), mixing between states is more substantial. The calculations also indicated that both complexes have a strong magnetic anisotropy, with Landé *g* factors that are fully axial for the ground doublet (g_z = 19.81, g_x = g_y = 0.00 for **1** and g_z = 19.80, g_x = g_y = 0.00 for **2**) and largely axial for the first excited doublet (g_z = 16.97, g_x = g_y = 0.02 for **1** and g_z = 16.95, g_x = 0.06, g_y = 0.07 for **2**), prompting investigation of the magnetic behavior of these compounds.

Compounds **1** and **2** were characterized in the solid state by static (dc) and dynamic (ac) magnetization measurements. The room temperature $\chi_M T$ values for **1** and **2** (13.75 emu·K·mol^{-1} and 13.64 emu·K·mol^{-1}, respectively) are slightly lower than the predicted value of 14.17 emu·K·mol^{-1} for an isolated Dy^{3+} ion ($^6H_{15/2}$, S = 5/2, L = 5, and g = 4/3), and are in excellent agreement with the *ab initio* calculated values of 13.78 emu·K·mol^{-1} for **1** and 13.80 emu·K·mol^{-1} for **2** (Figures S10 and S18). The decrease in $\chi_M T$ observed for both compounds upon lowering the temperature to 20 K is also fairly well reproduced by the calculations, providing further evidence that the ground state sub-level energies are accurately predicted, since this decrease in $\chi_M T$ reflects thermal depopulation of the crystal-field-split M_J levels. Below 20 K, $\chi_M T$ exhibits a marked decrease that differs from the predicted behavior, especially in the case of compound **1**. We attribute this decrease to the presence of strong dipolar interactions, which probably exist within both compounds, and may be expected to be stronger in **1** due to the shorter Dy···Dy distance.

Ac magnetic susceptibility measurements performed on **1** and **2** revealed peaks in the out-of-phase susceptibility (χ'') at temperatures up to 50 and 40 K, respectively, in the absence of an applied dc field. In the case of **2**, the low-temperature peaks exhibit little temperature dependence between 2 and 8 K, and as a result the Arrhenius plot of the relaxation times versus inverse temperature shows a plateau at the lowest temperatures (Figure S25). This temperature-independent behavior is consistent with quantum tunneling as the primary magnetic relaxation pathway at very low temperatures. At higher temperatures, the out-of-phase peaks for **2** shift markedly with temperature (Figure S20) and the Arrhenius plot shows a power dependent relationship with temperature, consistent with Raman relaxation. Even at the highest temperatures investigated, a clear linear regime expected for an Orbach relaxation process was not observed. This behavior remained for ac data collected under an applied dc field of 1200 Oe, determined to be the optimal field for slowing down the magnetic relaxation (Figure S23). Even still, we found it was not possible to fit the data using only Raman and quantum tunneling processes, and thus the temperature dependence of the relaxation times for **2** was fit using the following equation that includes Raman, Orbach and quantum tunneling contributions.

$$\tau^{-1} = CT^n + \tau_0^{-1}\exp(-U_{eff}/k_BT) + \tau_{tunnel}^{-1} \qquad \text{(Equation 1)}$$

For data collected under zero applied field, the resulting fit parameters are n = 3.54, C = 0.00603 s^{-1}·K^{-n}, τ_{tunnel} = 0.0427 s, τ_0 = 9.63 × 10^{-10} s, and U_{eff} = 336 cm^{-1}. Under a 1200 Oe dc field, n = 4.42 and C = 2.23 × 10^{-4} s^{-1}·K^{-n} while τ_0 and U_{eff} remained unchanged relative to the zero-field data. While the fitted relaxation barrier of 336 cm^{-1} agrees well with the energy of the first excited doublet determined by luminescence measurements (335 cm^{-1}) and reasonably well with *ab initio* calculations (282 cm^{-1}), other values of U_{eff} and τ_0 were also found to reproduce the evolution of relaxation times in the observed temperature range (Figure S25 and Table S13). Therefore, the lack of a clear linear regime in the relaxation data for **2** makes it impossible to definitively characterize the higher-temperature relaxation behavior.

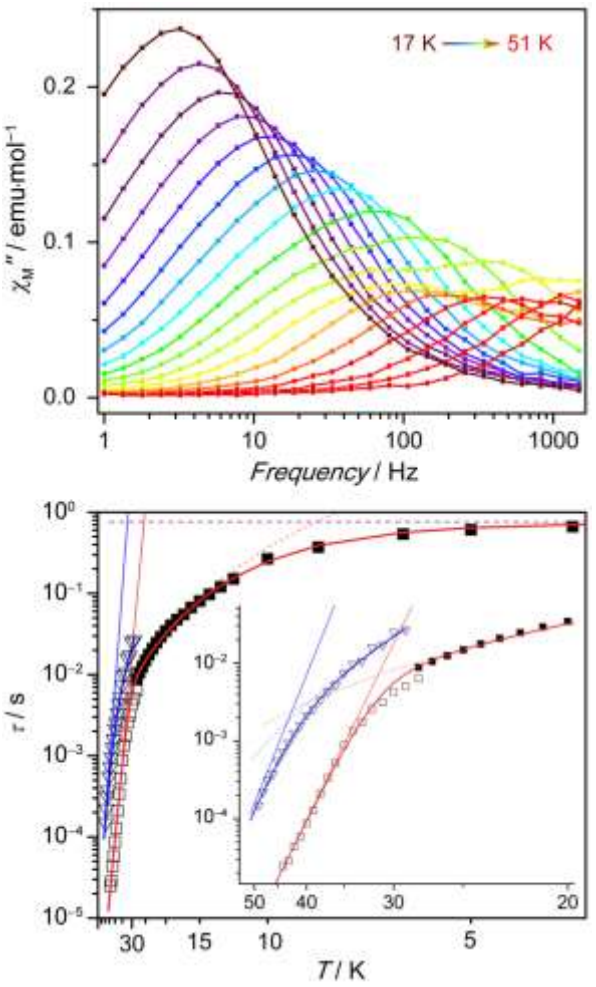

Figure 4. Out-of-phase magnetic susceptibility versus ac frequency under zero applied dc field and between 17 and 51 K for **1** (top). Relaxation times for **1** were extracted by fitting with a single process (black squares) or with two processes (open squares and triangles). Also shown are the best total fits for the two processes (solid red and blue lines), and decomposition of each fit into Raman (dotted lines), Orbach (solid lines), and quantum tunnelling (dashed line) contributions (bottom).

In the case of **1**, ac magnetic susceptibility data reveal slower and more complex relaxation behavior. The quantum tunneling process is much slower than that observed for **2**, with τ reaching a plateau around 0.7 s (Figure 4). Peaks arise in the

out-of-phase susceptibility and, above 28 K, two overlapping peaks become resolved, with the slower of the corresponding processes persisting up to 50 K within the 1-1500 Hz frequency range. Thus, for T > 28 K, extracting magnetic relaxation times required use of a two-component Debye model (see Table S9), and the resulting Arrhenius plot for **1** exhibits one relaxation time below 28 K and two relaxation times above 28 K. In contrast to compound **2**, a linear regime can clearly be observed for **1**, indicating the presence of an Orbach relaxation process. To fit this complex ac data, Equation 1 was first used to obtain a set of parameters corresponding to the faster relaxation regime, resulting in values of n = 3.46, C = 9.42 × 10^{-4} $s^{-1}\cdot K^{-n}$, τ_{tunnel} = 0.76 s, τ_0= 1.48 × 10^{-11} s, and U_{eff} = 432 cm^{-1} (Figure 4, red lines). The slower regime was then independently fit with the same equation using the following parameters: n = 9, C = 2.02 × 10^{-9} $s^{-1}\cdot K^{-n}$, τ_{tunnel}= 0.76 s, τ_0 = 2.82 × 10^{-10} s, and U_{eff} = 528 cm^{-1} (Figure 4, blue lines). The relaxation barrier of 432 cm^{-1} extracted for the fast regime is notably quite close to the energy of the second excited doublet determined by luminescence measurements (453 cm^{-1}) and *ab initio* calculations (477 cm^{-1}). Therefore, relaxation likely occurs by thermally-assisted quantum tunneling through the second excited doublet. This experimental observation indicates a highly axial first excited doublet with suppressed quantum tunneling, as supported by the *ab initio* calculations. For the slower relaxation regime, the relaxation barrier of 528 cm^{-1} extracted from the ac data is strikingly close to the position of the third excited doublet determined by luminescence measurements (527 cm^{-1}) and also agrees reasonably well with the value obtained from *ab initio* calculations (573 cm^{-1}). The assignment of this slowest process as a thermally-assisted quantum tunneling via the third excited doublet would not be unprecedented,[11f] but remains somewhat tentative owing to the absence of a distinct linear regime and the aforementioned low sensitivity of the fitting procedure to the barrier value in such a case.

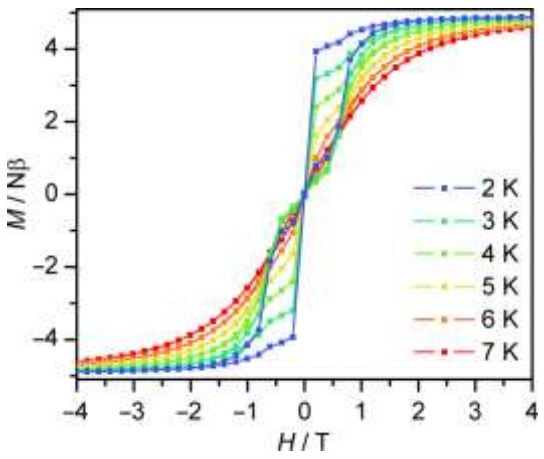

Figure 5. Hysteresis in the $M(H)$ curve for **1**, collected at temperatures ranging from 2 to 7 K with a 10 mTs^{-1} sweep rate.

Magnetic hysteresis was also observed in the magnetization versus field curves for both compounds, up to 7 and 4 K for **1** and **2**, respectively (Figures 5 and S27). Both compounds exhibit waist-restricted hysteresis loops, as expected due to the observed contribution of quantum tunneling at low temperatures in the zero-field ac susceptibility data.

To better understand the origins of magnetic blocking in these compounds, the transition probabilities between different sub-states were extracted from the *ab initio* calculations, without taking into account phonon-driven mechanisms.[7a, 14] Of particular interest is the fact that distinct relaxation behaviors were observed for the two compounds, despite their very similar crystal field splittings. Examining the probability of a transition from the first excited |+13/2> state in **2**, we find that both quantum tunnelling to the |−13/2> state and a phonon-assisted transition to |−11/2> are three times more probable than the same transitions in **1** (Figures 6 and S28). Likely, this difference arises due to the more distorted coordination sphere of the Dy^{III} complex in **2**. We thus ascribe the thermally-activated slow magnetic relaxation for **2** as occurring through the first excited state, in line with our experimental observation. In contrast, in compound **1** the probability of a transition becomes significant only for the |+11/2> state, and the calculation supports thermally-assisted quantum tunneling in the second excited doublet as the main mechanism for relaxation.

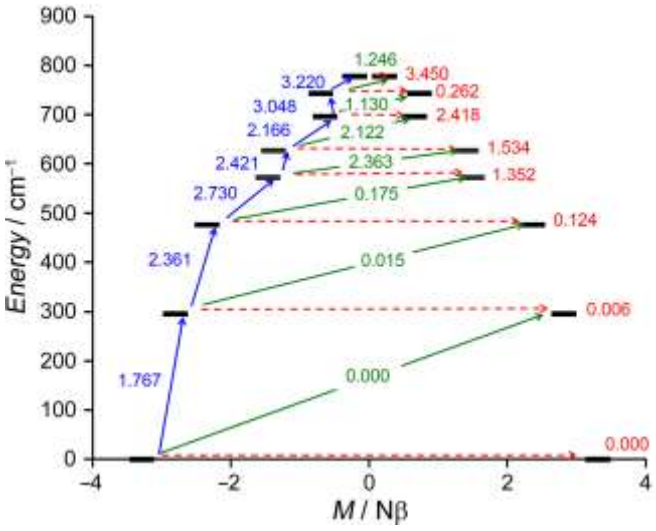

Figure 6. Calculated ground state splitting for **1** with the probability of transition between different sub-states, showing the most probable routes for magnetic relaxation in **1** (see SI for details).

In conclusion, we have presented the first Dy^{III} complexes bearing a terminal fluoride ligand, and explored the influence of this highly electrostatic metal–ligand interaction on the electronic structure. From the correlations between high-resolution luminescence data, results from magnetometry measurements, and *ab initio* calculations,[15] it is clear that such an architecture gives rise to a large crystal field splitting of the ground state and a pronounced axial magnetic anisotropy for the ground magnetic doublet, as well as for the first and second excited doublets for the more symmetrical complex in **1**. These air-stable complexes further exhibit slow relaxation of the magnetization, while compound **1** appears to relax through a large, multilevel barrier.

Our continued efforts are focused on fully realizing the potential of these highly anisotropic units by minimizing competing fast relaxation pathways, through suppression of dipolar coupling, isotopic enrichment,[16] or the introduction of an exchange interaction.[17]

Acknowledgements

This project received funding from the European Union's Horizon 2020 research and innovation program Marie Skłodowska Curie grant agreement N° 800719. We thank the French GENCI/IDRIS-CINES centre for high-performance computing resources and the U.S. National Science Foundation for support of the contributions of J.R.L., L.E.D., M.I.G, and K.C. through grant CHE-1464841. We further thank the NSF for graduate fellowship support of L.E.D. and Prof. A. P. Alivisatos for use of the fluorimeter. Single-crystal X-ray diffraction data were collected at Beamline 11.3.1 at the Advanced Light Source and the UC Berkeley Small Molecule X-ray Crystallography Facility (Chexray). The Advanced Light Source is supported by the Director, Office of Science, Office of Basic Energy Sciences, of the U. S. DOE under Contract No. DE-AC02-05CH11231. The ChexQuazar instrument used at the UC Berkeley Chexray facility is supported by an NIH Shared Instrumentation Grant S10-RR027172. Dr. K. R. Meihaus is thanked for editorial assistance.

Keywords: luminescence • single molecule magnet • ab initio calculations • crystal field slitting • lanthanide

[1] R. Sessoli, D. Gatteschi, A. Caneschi, M. A. Novak, *Nature* 1993, *365*, 141-143.

[2] a) D. Gatteschi, R. Sessoli, J. Villain, *Molecular Nanomagnets*, Oxford University Press, Oxford, **2006**; b) D. G. C. Benelli, *Introduction to Molecular Magnetism. From Transition Metals to Lanthanide.*, Wiley-VCH, Weinheim **2015**; c) G. A. Timco, S. Carretta, F. Troiani, F. Tuna, R. J. Pritchard, C. A. Muryn, E. J. L. McInnes, A. Ghirri, A. Candini, P. Santini, G. Amoretti, M. Affronte, R. E. P. Winpenny, *Nat. Nanotechnol.* **2009**, *4*, 173-178; d) S. G. McAdams, A.-M. Ariciu, A. K. Kostopoulos, J. P. S. Walsh, F. Tuna, *Coord. Chem. Rev.* **2017**, *346*, 216-239; e) S. T. Liddle, J. van Slageren, *Chem. Soc. Rev.* **2015**, *44*, 6655-6669; f) F. Pointillart, O. Cador, B. Le Guennic, L. Ouahab, *Coord. Chem. Rev.* **2017**, *346*, 150-175; g) S. Demir, I.-R. Jeon, J. R. Long, T. D. Harris, *Coord. Chem. Rev.* **2015**, *289*, 149-176; h) Y.-S. Meng, S.-D. Jiang, B.-W. Wang, S. Gao, *Acc. Chem. Res.* **2016**, *49*, 2381-2389.

[3] a) N. Ishikawa, M. Sugita, T. Ishikawa, S. Koshihara, Y. Kaizu, *J. Am. Chem. Soc.* **2003**, *125*, 8694-8695; b) N. Ishikawa, Y. Mizuno, S. Takamatsu, T. Ishikawa, S. Y. Koshihara, *Inorg. Chem.* **2008**, *47*, 10217-10219.

[4] a) N. F. Chilton, D. Collison, E. J. L. McInnes, R. E. P. Winpenny, A. Soncini, *Nat. Commun.* **2013**, *4:*2551; b) J. D. Rinehart, J. R. Long, *Chem. Sci.* **2011**, *2*, 2078-2085; c) L. Ungur, L. F. Chibotaru, *Chem. Eur. J.* **2017**, *23*, 3708-3718; d) J. Luzon, R. Sessoli, *Dalton Trans.* **2012**, *41*, 13556-13567.

[5] a) L. Ungur, L. F. Chibotaru, *Inorg. Chem.* **2016**, *55*, 10043-10056; b) N. F. Chilton, *Inorg. Chem.* **2015**, *54*, 2097-2099.

[6] a) J. Liu, Y.-C. Chen, J.-L. Liu, V. Vieru, L. Ungur, J.-H. Jia, L. F. Chibotaru, Y. Lan, W. Wernsdorfer, S. Gao, X.-M. Chen, M.-L. Tong, *J. Am. Chem. Soc.* **2016**, *138*, 5441-5450. b) Y.-S. Ding, N. F. Chilton, R. E. P. Winpenny, Y.-Z. Zheng, *Angew. Chem. Int. Ed.* **2016**, *55*, 16071-16074. c) S. K. Gupta, T. Rajeshkumar, G. Rajaraman, R. Murugavel, *Chem. Sci.* **2016**, *7*, 5181-5191.

[7] a) C. A. P. Goodwin, F. Ortu, D. Reta, N. F. Chilton, D. P. Mills, *Nature* **2017**, *548*, 439-442; b) F.-S. Guo, B. M. Day, Y.-C. Chen, M.-L. Tong, A. Mansikkamäki, R. A. Layfield, *Angew. Chem. Int. Ed.* **2017**, *56*, 11445-11449.

[8] K. S. Pedersen, M. A. Sørensen, J. Bendix, *Coord. Chem. Rev.* **2015**, *299*, 1-21.

[9] a) A. C. Hillier, Zhang, G. H. Maunder, S. Y. Liu, T. A. Eberspacher, M. V. Metz, R. McDonald, Â. Domingos, N. Marques, V. W. Day, A. Sella, J. Takats, *Inorg. Chem.* **2001**, *40*, 5106-5116; b) U. J. Williams, J. R. Robinson, A. J. Lewis, P. J. Carroll, P. J. Walsh, E. J. Schelter, *Inorg. Chem.* **2014**, *53*, 27-29; c) M. L. Cole, G. B. Deacon, C. M. Forsyth, P. C. Junk, K. Konstas, J. Wang, *Chem. Eur. J.* **2007**, *13*, 8092-8110; d) P. L. Watson, T. H. Tulip, I. Williams, *Organometallics* **1990**, *9*, 1999-2009; e) O. A. Blackburn, A. M. Kenwright, A. R. Jupp, J. M. Goicoechea, P. D. Beer, S. Faulkner, *Chem. Eur. J.* **2016**, *22*, 8929.

[10] a) P. L. Jones, A. J. Amoroso, J. C. Jeffery, J. A. McCleverty, E. Psillakis, L. H. Rees, M. D. Ward, *Inorg. Chem.* **1997**, *36*, 10-18; b) A. J. Amoroso, A. M. C. Thompson, J. C. Jeffery, P. L. Jones, J. A. McCleverty, M. D. Ward, *J. Chem. Soc., Chem. Commun.* **1994**, 2751-2752.

[11] a) Y. Bi, C. Chen, Y.-F. Zhao, Y.-Q. Zhang, S.-D. Jiang, B.-W. Wang, J.-B. Han, J.-L. Sun, Z.-Q. Bian, Z.-M. Wang, S. Gao, *Chem. Sci.* **2016**, *7*, 5020-5031; b) G. Cucinotta, M. Perfetti, J. Luzon, M. Etienne, P.-E. Car, A. Caneschi, G. Calvez, K. Bernot, R. Sessoli, *Angew. Chem. Int. Ed.* **2012**, *51*, 1606-1610; c) S. Chorazy, M. Rams, K. Nakabayashi, B. Sieklucka, S.-i. Ohkoshi, *Chem. Eur. J.* **2016**, *22*, 7371-7375; d) M. Al Hareri, Z. Ras Ali, J. Regier, E. L. Gavey, L. D. Carlos, R. A. S. Ferreira, M. Pilkington, *Inorg. Chem.* **2017**, *56*, 7344-7353; e) E. Mamontova, J. Long, R. Ferreira, A. Botas, D. Luneau, Y. Guari, L. Carlos, J. Larionova, *Magnetochemistry* **2016**, *2*, 41; f) M. Gregson, N. F. Chilton, A.-M. Ariciu, F. Tuna, I. F. Crowe, W. Lewis, A. J. Blake, D. Collison, E. J. L. McInnes, R. E. P. Winpenny, S. T. Liddle, *Chem. Sci.* **2016**, *7*, 155-165; g) S. Shintoyo, K. Murakami, T. Fujinami, N. Matsumoto, N. Mochida, T. Ishida, Y. Sunatsuki, M. Watanabe, M. Tsuchimoto, J. Mrozinski, C. Coletti, N. Re, *Inorg. Chem.* **2014**, *53*, 10359-10369; h) Q.-W. Li, J.-L. Liu, J.-H. Jia, J.-D. Leng, W.-Q. Lin, Y.-C. Chen, M.-L. Tong, *Dalton Trans.* **2013**, *42*, 11262-11270.

[12] A. Ruiz-Martínez, D. Casanova, S. Alvarez, *Chem. Eur. J.* **2008**, *14*, 1291-1303..

[13] S. V. B. Eliseeva, J.C.G. Bunzli, *Chem.Soc. Rev.* **2010**, *39*, 189-227

[14] A. Lunghi, F. Totti, R. Sessoli, S. Sanvito, *Nat. Commun.* **2017**, *8*, 14620.

[15] a) K. S. Pedersen, J. Dreiser, H. Weihe, R. Sibille, H. V. Johannesen, M. A. Sørensen, B. E. Nielsen, M. Sigrist, H. Mutka, S. Rols, J. Bendix, S. Piligkos, *Inorg. Chem.* **2015**, *54*, 7600-7606; b) F. Pointillart, B. Le Guennic, S. Golhen, O. Cador, O. Maury, L. Ouahab, *Chem. Commun.* **2013**, *49*, 615-617; c) X. Yi, K. Bernot, V. Le Corre, G. Calvez, F. Pointillart, O. Cador, B. Le Guennic, J. Jung, O. Maury, V. Placide, Y. Guyot, T. Roisnel, C. Daiguebonne, O. Guillou, *Chem. Eur. J.* **2014**, *20*, 1569-1576; d) G. Cosquer, F. Pointillart, J. Jung, B. Le Guennic, S. Golhen, O. Cador, Y. Guyot, A. Brenier, O. Maury, L. Ouahab, *Eur. J. Inorg. Chem.* **2014**, *2014*, 69-82.

[16] F. Pointillart, K. Bernot, S. Golhen, B. Le Guennic, T. Guizouarn, L. Ouahab, O. Cador, *Angew. Chem. Int. Ed.* **2015**, *54*, 1504-1507.

[17] J. D. Rinehart, M. Fang, W. J. Evans, J. R. Long, *Nat. Chem.* **2011**, *3*, 538-542.

10.1002/anie.201712139

Entry for the Table of Contents (Please choose one layout)
Layout 1:

COMMUNICATION

A strong donor terminal fluoride ligand generates large crystal field splittings within dysprosium(III) complexes and give rise to new air stable single molecule magnets with large barriers to magnetic relaxation.

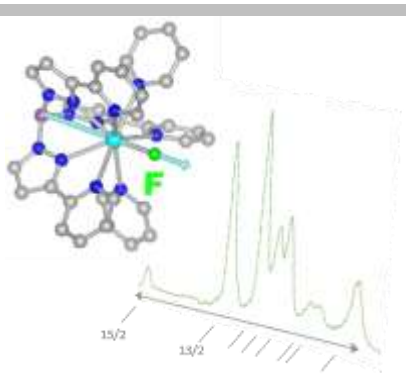

Dr. Lucie Norel,* Lucy E. Darago, Dr. Boris Le Guennic, Khetpakorn Chakarawet, Miguel I. Gonzalez, Dr. Jacob H. Olshansky, Prof. Stéphane Rigaut and Prof. Jeffrey R. Long*

Page No. – Page No.

A Terminal Fluoride Ligand Generates Highly Axial Magnetic Anisotropy in Dysprosium Complexes